ACCOUNTS of chemical research

pubs.acs.org/accounts Article

# Constructing Pure Si Anodes for Advanced Lithium Batteries

Minjun Je,[§] Dong-Yeob Han,[§] Jaegeon Ryu,* and Soojin Park*

Cite This: *Acc. Chem. Res.* 2023, 56, 2213−2224 Read Online

ACCESS | Metrics & More | Article Recommendations

**CONSPECTUS:** With the escalating demands of portable electronics, electric vehicles, and grid-scale energy storage systems, the development of next-generation rechargeable batteries, which boasts high energy density, cost effectiveness, and environmental sustainability, becomes imperative. Accelerating these advancements could substantially mitigate detrimental carbon emissions. The pursuit of main objectives has kindled interest in pure silicon as a high-capacity electroactive material, capable of further enhancing the gravimetric and volumetric energy densities compared with traditional graphite counterparts. Despite such promising attributes, pure silicon materials face significant hurdles, primarily due to their drastic volumetric changes during the lithiation/delithiation processes. Volume changes give rise to severe side effects, such as fracturing, pulverization, and delamination, triggering rapid capacity decay. Therefore, mitigating silicon particle fracture remains a primary challenge. Importantly, nanoscale silicon (below 150 nm in size) has shown resilience to stresses induced by repeated volume changes, thereby highlighting its potential as an anode-active material. However, the volume expansion stress not only affects the internal structure of the particle but also disrupts the solid−electrolyte interphase (SEI) layer, formed spontaneously on the outer surface of silicon, causing adverse side reactions. Therefore, despite silicon nanoparticles offering new opportunities, overcoming the associated issues is of paramount importance.

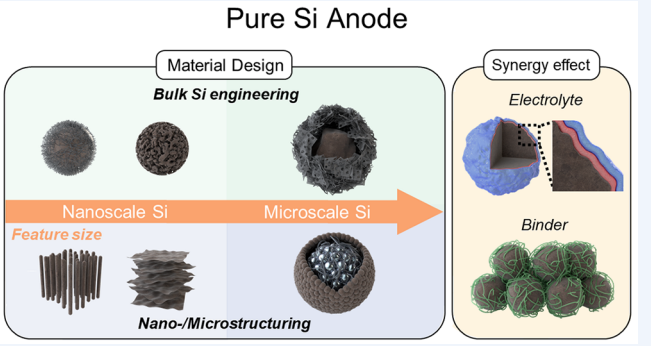


Thus, this Account aims to spotlight the significant strides made in the development of pure silicon anodes with particular attention to feature size. From the emergence of nanoscale silicon, the following nanotechnology played a crucial role in growing the particle through nano/microstructuring. Similarly, bulk silicon microparticles gradually surfaced with the post-engineering methods owing to their practical advantages. We briefly discuss the special characteristics of representative examples from bulk silicon engineering and nano/microstructuring, all aimed at overcoming intrinsic challenges, such as limiting large volume changes and stabilizing SEI formation during electrochemical cycling. Subsequently, we outline guidelines for advancing pure silicon anodes to incorporate high mass loading and high energy density. Importantly, these advancements require superior material design and the incorporation of exceptional battery components to ensure compatibility and yield synergistic effects. By broadening the cooperative strategies at the cell and system levels, we anticipate that this Account will provide an insightful analysis of pure silicon anodes and catalyze their practical applications in real battery systems.

## KEY REFERENCES

- Lee, J.-I.; Ko, Y.; Shin, M.; Song, H.-K.; Choi, N.-S.; Kim, M. G.; Park, S. High-performance silicon-based multicomponent battery anodes produced via synergistic coupling of multifunctional coating layers. *Energy Environ. Sci.* **2015**, *8*, 2075−2084.[1] This paper reports a dual-component coating layer on Si nanoparticles to obtain good mechanical properties and improved conductivities.
- Ryu, J.; Chen, T.; Bok, T.; Song, G.; Ma, J.; Hwang, C.; Luo, L.; Song, H.-K.; Cho, J.; Wang, C.; Zhang, S.; Park, S. Mechanical mismatch-driven rippling in carbon-coated silicon sheets for stress-resilient battery anodes. *Nat. Commun.* **2018**, *9*, 2924.[2] This work reveals distinctive structural characteristics of 2D Si nanosheets through in situ experiments. The rippling morphology significantly reduced internal stress during cycles and improved mechanical durability.
- Ryu, J.; Seo, J. H.; Song, G.; Choi, K.; Hong, D.; Wang, C.; Lee, H.; Lee, J. H.; Park, S. Infinitesimal sulfur fusion yields quasi-metallic bulk silicon for stable and fast energy storage. *Nat. Commun.* **2019**, *10*, 2351.[3] This approach formed quasi-metallic silicon microparticles by

Received: May 30, 2023
Published: August 1, 2023





https://doi.org/10.1021/acs.accounts.3c00308
*Acc. Chem. Res.* 2023, 56, 2213−2224

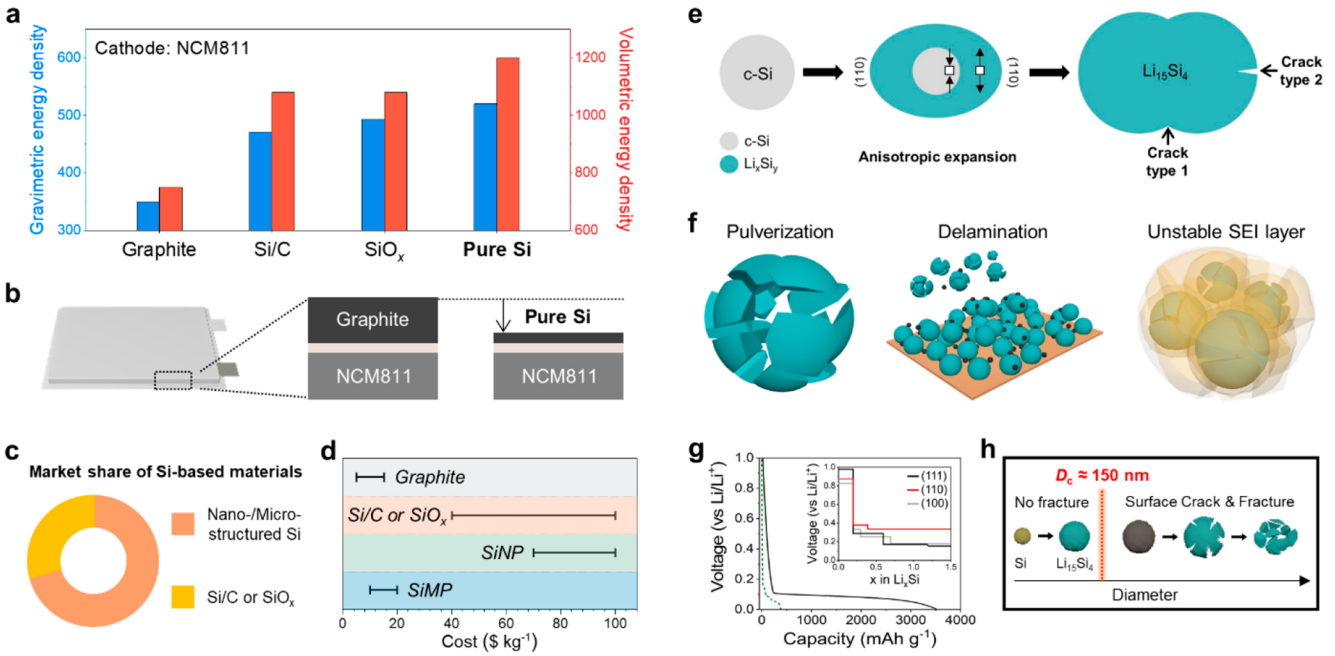


**Figure 1.** Basic characteristics of the pure Si anode. (a) Practical gravimetric and volumetric energy densities of graphite, Si/C, $SiO_x$, and pure Si anodes paired with the NCM811 cathode at the cell level (unit: Wh $kg^{-1}$ and Wh $L^{-1}$ for gravimetric energy density and volumetric energy density, respectively.) (b) Comparison of the cell thickness between graphite|NCM811 and pure Si|NCM811. (c) Current market share of Si-based materials and (d) cost comparison of graphite, Si/C or $SiO_x$, pure SiNP, and pure SiMP. (e) Schematic diagram for volumetric expansion, the anisotropic property, and crack formation of crystalline Si during the lithiation process. (f) Main degradation mechanism of Si anodes originates from the large volume expansion of Si during lithiation. (g) Electrochemical lithiation curves of Si (black solid line) and graphite (green dashed line) anodes (inset: DFT voltage profiles for the lithiated reaction into each (111), (110), and (111) plane of crystalline Si). Adapted with permission from ref 15. Copyright 2011 American Chemical Society. (h) Critical size ($D_c$) for occurring particle fracture upon lithiation and volume expansion.

small amounts of sulfur doping. The flexible and robust sulfur-supported channels facilitated highly stable battery cycling at a fast charging rate with a high energy density.

- Je, M.; Song, G.; Lee, S.; Park, H. J.; Kim, J.; Park, S. Practical production of heteroatom-bridged and mixed amorphous−crystalline silicon for stable and fast-charging batteries. *J. Mater. Chem. A* **2023**, *11*, 1694−1703.[4] This work constructed mixed amorphous−crystalline silicon microparticles with localized heteroatom bridges in a silicon crystal from borosilicate glass. A cost-effective, scalable synthetic system demonstrated the feasibility of practical production for stable and fast-charging pure silicon anodes.

## 1. INTRODUCTION

The advent of secondary batteries has ushered in a new era, and the demand for electric vehicles has increased with the rapid development of lithium ion batteries (LIBs).[5] In addition, green policies have emerged to promote sustainable development by encouraging the replacement of traditional energy sources with rechargeable batteries.[6] Despite graphite being the most commonly used anode material in commercial LIBs, it has a low theoretical capacity of 372 mAh $g^{-1}$, of which the available capacity has almost reached the theoretical limit in the battery industry. As a result, even when paired with a high-voltage cathode ($LiNi_{0.8}Co_{0.1}Mn_{0.1}O_2$, NCM811) (Figure 1a), the energy density of graphite anodes falls far short of market demand.[7] Therefore, it is essential to discover new anode materials to overcome this energy density bottleneck.

Silicon (Si) has emerged as an alternative anode material for next-generation batteries due to its high theoretical capacity (3579 mAh $g^{-1}$ for $Li_{15}Si_4$) and low operating voltage (<0.4 V versus $Li/Li^+$), offering much higher energy density than that of conventional graphite anodes.[8] Full cells using the Si anode in the form of either $SiO_x$ ($0 < x < 2$) or Si/C paired with NCM811 cathodes have demonstrated gravimetric energy densities of 471 and 493 Wh $kg^{-1}$, respectively.[9] Instead, employing pure Si (anode comprising 100% Si) in practical cells can further increase the gravimetric energy densities up to 520 Wh $kg^{-1}$. Similarly, full cells with Si/C and $SiO_x$ anodes exhibit notably higher volumetric energy density of 1080 Wh $L^{-1}$ compared with graphite-based cells (750 Wh $L^{-1}$). Importantly, the utilization of a pure Si anode can maximize the volumetric energy density up to 1200 Wh $L^{-1}$.[10] This allows for high mass loading with a pure Si ultrathin film electrode compared to a conventional graphite anode with the same areal capacity (Figure 1b). Thanks to the aforementioned energy density advantages, Si-based materials already occupy a significant share in the market, with nano/microstructured Si and Si/C or $SiO_x$ (Figure 1c).[11] As depicted in Figure 1d, the choice of materials is primarily affected by the inherent structural instability of Si, which has led to the adoption of comparatively improved materials.[12,13] While cost considerations certainly come into play, the main concern remains the enhancement of the intrinsic stability.

High Li stoichiometry of Si enables the accommodation of 3.75 Li atoms per Si based on the Li-alloying mechanism at room temperature, which inevitably causes enormous volume changes (>300%) during battery cycling.[14] Therefore, the


https://doi.org/10.1021/acs.accounts.3c00308
Acc. Chem. Res. 2023, 56, 2213−2224

accumulated internal stress causes particle fracture and pulverization, ending with an unsatisfactory cycle life (Figure 1e). The lithiation/delithiation process leads to two types of cracks. First, crystalline Si possesses different energy barriers toward Li insertion at each plane.[15] The characteristic promotes preferential lithiation on a specific plane (i.e., (110) plane) at an early stage, yielding anisotropic expansion and consequent surface cracking between locally expanded (110) planes (Figure 1g).[16,17] Second, stress reversal is observed at the core−shell-type interface between the unlithiated Si phase and the lithiated Si ($Li_xSi_y$) phase in individual Si particles during electrochemical cycling. Such volumetric expansion contributes to the progression of crack growth, inducing pulverization and delamination issues (Figure 1f). Simultaneously, a rupture in the SEI layer unveils new surfaces, triggering continuous side reactions with the electrolyte, which in turn leads to the formation of a thick SEI layer with a high impedance.[18] The resultant problems instigate a fast capacity decay due to the loss of active material. In the meantime, several studies found that this hoop stress is proportional to the feature size of the host material. When accounting for the stress state as well as lithiation-induced swelling and associated plasticity, the Si particle can withstand the resulting stress for itself under a threshold particle size of <150 nm (Table 1 and Figure 1h).[19−23] Nanosized Si, capable of tolerating mechanical stress, suggested the viability of utilizing pure Si as an anode material, triggering the onset of extensive research.

**Table 1. Young's Modulus and Yield Point of Si Materials**

| Material | Description | Value (GPa) | refs |
|---|---|---|---|
| Crystalline Si | Young's modulus | 185 | 20 |
| | Yield point | 7 | 21 |
| $Li_xSi_y$ alloy | Young's modulus | 35 | 22 |
| | Yield point | 1 | 23 |

In recent decades, considerable advancements have been made in the development of pure Si anodes, primarily beginning with revolutionary strides in reducing the feature size. These significant strides can largely be classified into two main categories: bulk Si engineering and nano/microstructuring. Furthermore, an explanation of the transition in feature size from the nanoscale to the microscale is presented, along with the unique characteristics of each Si structure. This Account aims to provide a comprehensive understanding and future research focal points for high-performance pure Si anodes by examining how the two categories have addressed the aforementioned challenges regarding the feature size of pure Si materials.

## 2. PROGRESS IN NANOSCALE FEATURE SIZE FOR THE PURE SI ANODE

Si electroactive materials with a particle size below 150 nm are capable of avoiding fracture due to insufficient strain to initiate and propagate crack growth. While Si nanoparticles (SiNPs) exhibit promising attributes, their cycle life remains constrained by inherently poor electrical conductivity and the instability of the SEI layer.[24]

### 2.1. Constructing the Si Nanoparticle Anode

To compensate for the conductivity issue, porous SiNP was adopted due to its high specific area, which not only offers an increased number of reaction sites for charge carriers during lithiation/delithiation but also ensures comparatively shorter diffusion pathway across the pores (Figure 2a).[25] Zhou et al. reported the preparation of porous Si particles as engineered from bulk metallurgical Si, known to contain metal impurities such as iron and aluminum. The removal of these elements supports the formation of a porous structure. In terms of

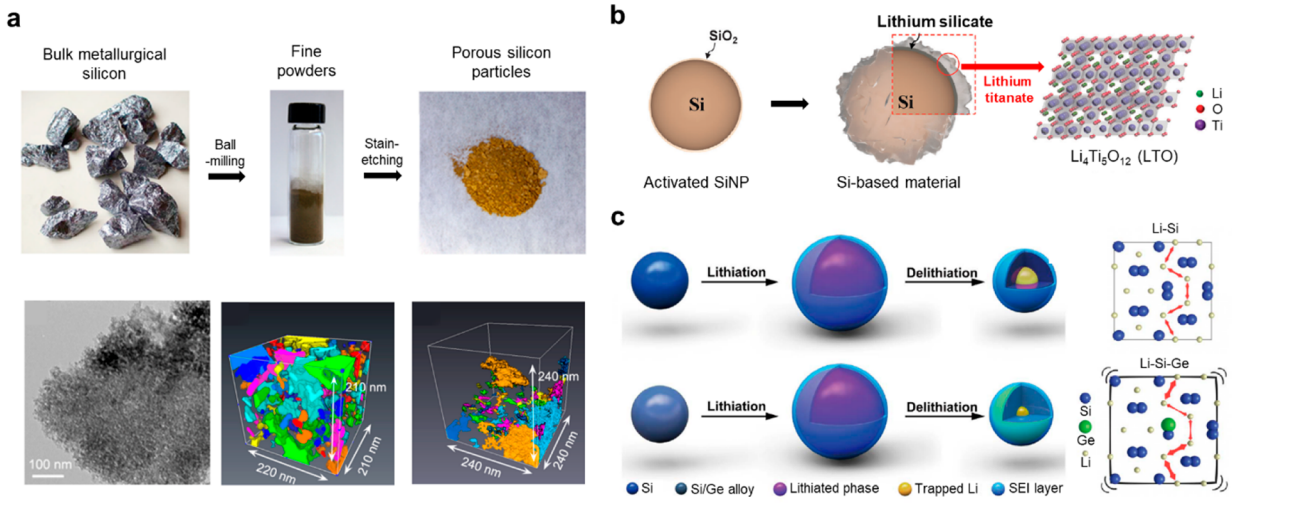


**Figure 2.** Bulk Si engineering for the advanced SiNP anode. (a) Synthetic route of porous Si from metallurgical Si through ball-milling, stain-etching, the corresponding TEM image of porous Si particles, and HAADF-STEM tomography. Labeled colors indicate the separated pore connections. Reproduced with permission from ref 25. Copyright 2014 American Chemical Society. (b) Schematic illustration showing the synthetic process of the Si-based materials@LTO. Reproduced with permission from ref 1. Copyright 2015 the authors. Published by Royal Society of Chemistry under a Creative Commons Attribution-NonCommercial 3.0 Unported (CC BY-NC 3.0) License. (c) Schematic of the lithiation/delithiation process (left) and Li diffusion (right) in the Si anode and Ge-doped Si anode. Reproduced with permission from ref 30. Copyright 2019 the authors. Published by American Association for the Advancement of Science under a Creative Commons Attribution-NonCommercial 4.0 International (CC BY-NC 4.0) License.



https://doi.org/10.1021/acs.accounts.3c00308
Acc. Chem. Res. 2023, 56, 2213−2224

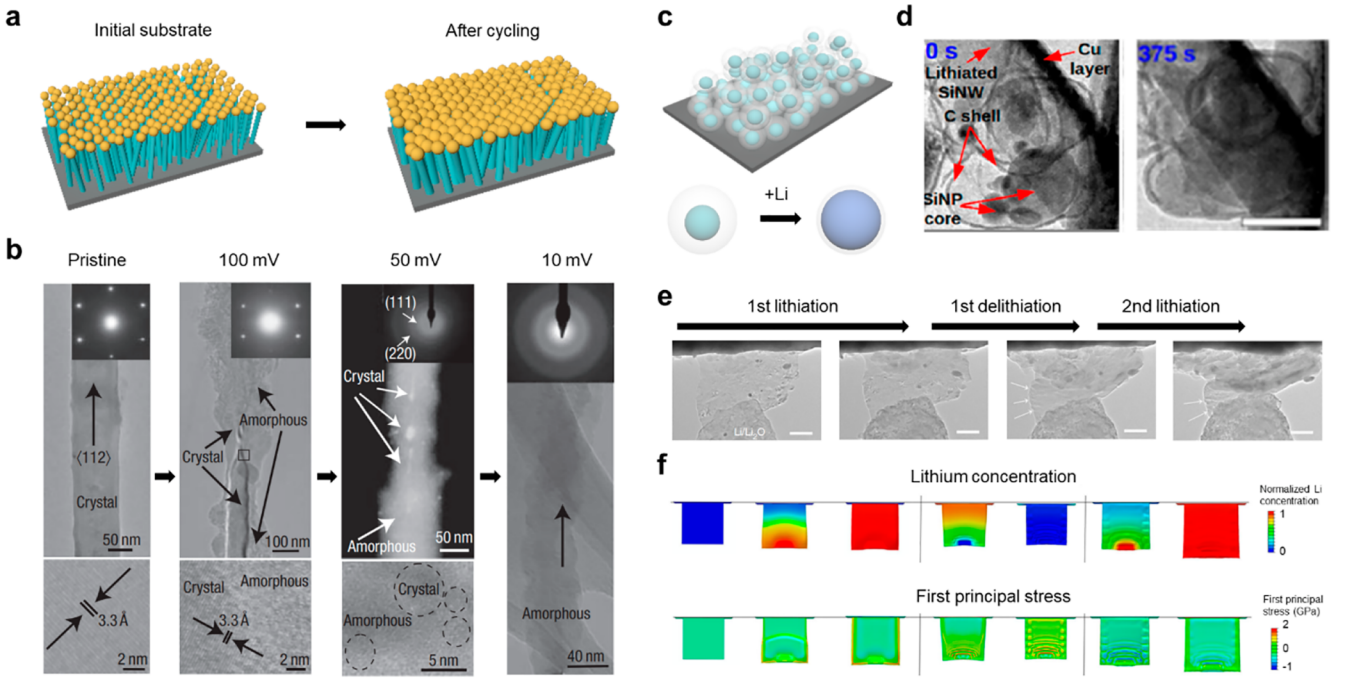


**Figure 3.** Nanostructuring for the advanced nanoscale Si anodes. (a) Schematic of morphological changes that occur in SiNWs during electrochemical cycling. (b) TEM data for SiNWs at different stages of the first charge. Reproduced with permission from ref 33. Copyright 2008 Springer Nature. (c) Schematic illustration of the Si@void@C electrode and magnified schematic of an individual Si@void@C particle showing that SiNP expands without breaking the carbon coating or disrupting the SEI layer on the outer surface. (d) In situ TEM images of Si@void@C in a pristine state (0 s) and after full lithiation. Adapted with permission from ref 34. Copyright 2012 American Chemical Society. (e) Time-lapse in situ TEM images of 2DSi@C and (f) snapshots of deformation morphologies predicted by the chemomechanical model for two lithiation cycles. Reproduced with permission from ref 2. Copyright 2018 the authors. Published by Springer Nature under a Creative Commons Attribution 4.0 International (CC BY 4.0) License.

employing Si particles as an active material, the ball-milling process stands as a common processing method for decreasing the feature size, generating nanoscale Si in the form of a fine powder. The porous structure evolved with the subsequent strain-etching process, using different etchants that influenced the degrees of porosity. A highly porous structure throughout the entire particle showed even better cycling performance, as sufficient pores reduce the bottleneck effect of Li-ion accumulation on the surface.[26] Notably, the plentiful pores and void spaces can alleviate the spatially volumetric change at both particle and electrode levels, minimizing the external and internal stresses that lead to irreversible deformation and consequently reinforcing structural integrity.

While a highly porous structure displayed superior resilience to crack formation and pulverization, challenges with the unstable SEI layer persist. The enlarged surface can exacerbate adverse reactions with organic electrolytes.[27] Therefore, coating strategies have been proposed to avoid such side reactions by creating a physical barrier at the interface that prevents direct interaction between the electrolyte and the Si surface (Figure 2b).[1] Our group proposed synergistic coupling of the multifunctional shell layers consisting of lithium silicate ($Li_2SiO_3$ and $Li_2Si_2O_5$) and lithium titanate ($Li_4Ti_5O_{12}$) stacked up on the Si surface. Mechanically strong lithium silicate plays a pivotal role as a self-buffering layer and mitigates volumetric changes, suppressing structural collapse. Notably, $Li_4Ti_5O_{12}$ was converted to a rock-salt $Li_7Ti_5O_{12}$ phase during the lithiation, which can facilitate fast Li-ion transport due to a three-dimensional (3D) network of ionic channels, and the electrochemically modified layer significantly enhanced the electrical conductivity, unlike an insulating $Li_4Ti_5O_{12}$. Consequently, the resulting stacked layers promoted the formation of a robust and stable SEI layer by restraining mechanical strain and stress caused by the repetitive volume change of Si and the bottleneck effect of Li-ion accumulation on the outer surface. The superior layer ensured a remarkably extended cycle life and reliable electrode integrity at a fast charging system.

In the meantime, doping or alloying strategies have been adopted to improve the electrical conductivities of Si in various fields. Infinitesimal amounts of heteroatom infusion in the crystal plane of Si alter the electronic band structure and density of states, which provides quasi-metallic properties and the lattice expansion that helps the facile transport of charge carriers. A computational chemistry approach was utilized to investigate the changes in Li insertion energy ($E_{insertion}$) under doping with different impurities, where $E_{insertion}$ becomes positive or negative depending on the dopant.[28] Interestingly, $E_{insertion}$ for B-doped Si is a negative value, indicating that Li insertion into Si is energetically favorable. However, P-doped Si, which has positive $E_{insertion}$, implies that the Li insertion reaction is energetically unfavorable. Therefore, the doping strategy can significantly affect the ease of lithium insertion into Si.[29] Cui et al. suggested that doping or alloying was obtained by controlling the ratio of Si to germanium (Ge) through the ball-milling process (Figure 2c).[30] Mechanical energy generated during the ball-milling process can be transformed into thermal energy and other forms, thereby effectively enhancing the solid-state chemical reactivity. Ge substitution in the Si crystal lattice leads to local volume


https://doi.org/10.1021/acs.accounts.3c00308
Acc. Chem. Res. 2023, 56, 2213−2224

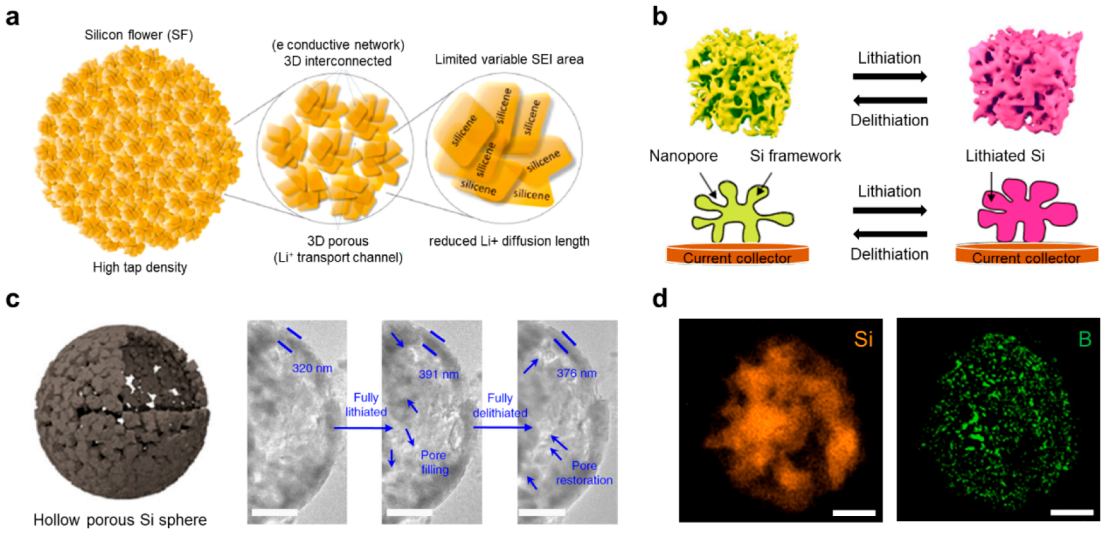


**Figure 4.** Microstructuring for the advanced microscale Si anode. (a) Schematic of silicene flowers features high tap density, three-dimensional electron/lithium ion transport channels, reduced lithium ion diffusion length, and limited variable SEI. Reproduced with permission from ref 37. Copyright 2017 American Chemical Society. (b) Schematic illustrating the lithiation/delithiation process of the ant-nest-like microscale porous Si particles showing inward volume expansion and stable Si framework retention during cycling. Reproduced with permission from ref 43. Copyright 2019 the authors. Published by Springer Nature under a Creative Commons Attribution 4.0 International (CC BY 4.0) License. (c) Schematic illustration of a hollow porous Si sphere (HPSS) and magnified TEM images of pristine, fully lithiated, and delithiated HPSS@C particles, which illustrate a thickened shell (22% expansion after lithiation) and pore filling/restoration showing no structural collapse. Reproduced with permission from ref 45. Copyright 2018 the authors. Published by Springer Nature under a Creative Commons Attribution 4.0 International (CC BY 4.0) License. (d) Electron energy loss spectroscopy (EELS) elemental mapping of mixed amorphous−crystalline Si (MACS) for Si (orange) and boron (green). Reproduced with permission from ref 4. Copyright 2023 Royal Society of Chemistry.

expansion or contraction within the diffusion channels depending on the relative positions owing to the larger ionic radius of Ge compared to that of Si. Therefore, the energy barrier for lithium diffusion varies with the extent of Ge substitution and achieved the minimum at a Ge concentration of 6.25 atom %.

## 2.2. Constructing the Nanostructured Si Anode

The engineering of SiNPs still could not solve several challenges, including relatively low electrical conductivity and poor stress management. To address these issues, various multidimensional nanostructuring strategies of Si have been proposed from one-dimensional (1D) to 3D structures.[31,32] The nanostructures offer higher degree of connectivity, facilitating better electronic percolation throughout the electrodes compared with the zero-dimensional SiNPs. Additionally, nanostructured Si provides a more interconnected and continuous framework that enhances the structural integrity, enabling better accommodation of the volume expansion through spatial engineering and mitigating mechanical degradation.

As a 1D nanostructure, Cui and co-workers introduced Si nanowires (SiNWs) as LIB anodes, which were directly grown onto a stainless-steel current collector using the vapor−liquid−solid growth mechanism (Figure 3a).[33] The SiNW electrode, designed with sufficient space between the wires, can alleviate the volume expansion. Intrinsic properties of SiNWs, such as large specific surface areas and short diffusion paths for charge carriers, contribute to internal stress reduction by radial and axial expansion. Additionally, the direct growth of the SiNWs onto the current collector ensured good electrical conductivity, facilitated by 1D conductive paths between the active material and the current collector. The structural evolution of SiNWs during the first Li insertion was investigated by transmission electron microscopy (TEM) and selected area electron diffraction (SAED) (Figure 3b). When the SiNW was charged to 100 mV, a crystalline core and an amorphous shell structure were clearly observed across the diameter. The SAED was also consistent with the TEM image, which showed the spot pattern for the crystalline phase (Si) and weak diffuse rings from the amorphous phase ($Li_xSi$ alloy). At 50 mV, the SiNW was mostly amorphous with some crystalline Si regions embedded within the core. Then, all of the Si had changed to amorphous $Li_{4.4}Si$ at 10 mV, as confirmed by the presence of amorphous rings in the SAED. This work suggests a novel approach to obtaining a beneficial nanostructure for the enhanced performance of pure Si anodes.

Although the Si NWs have demonstrated high resistance to pulverization and moderate ionic/electrical conductivity, the SEI remains unstable due to outward expansion during lithiation. To construct a stable interphase, a yolk−shell structure was designed where the SiNPs (≈ 100 nm) as the "yolk" and amorphous carbon (5−10 nm thick) served as the "shell" (Figure 3c).[34] Each Si yolk is anchored on one side of the carbon shell, leaving an 80−100 nm void space on the opposite side. The intentionally introduced void space between SiNPs and the carbon shell suppresses the volume change during lithiation without breaking the carbon shell. The structural stability of the yolk−shell allows for the construction of a robust SEI on the surface of the carbon shell while preventing the repetitive rupturing and reformation of the SEI. In situ TEM unveiled that a fracture was not observed in the Si cores upon complete lithiation, and the carbon shell remains intact, which confirmed the structural advantages of the yolk−shell design (Figure 3d).

As another approach, two-dimensional (2D) Si nanosheets have been employed as anode materials in LIBs, which allows facile accessibility of Li ions through a larger surface area and


https://doi.org/10.1021/acs.accounts.3c00308
Acc. Chem. Res. 2023, 56, 2213−2224

mitigates the volume expansion owing to the spatial characteristic of 2D.[35] 2D Si nanosheets conformally coated with amorphous carbon layers (2DSi@C) were reported which significantly reduced the internal stress by the rippling phenomena.[2] The nonporous structure of 2DSi@C enables the formation of a stable SEI layer without further consumption of electrolyte, which achieved a high initial Coulombic efficiency of 92.3%. The structural deformation morphology of 2DSi@C in the first two cycles was monitored by in situ TEM (Figure 3e). It was observed that 2DSi@C underwent anisotropic swelling of 9.7 and 200% in the lateral and thickness directions, respectively, during the first lithiation. Notably, the flake was crumpled, with prominent ripples propagating along the lithiation direction during the delithiation. Upon secondary lithiation, the ripples became flattened while maintaining their 2D morphology without fracture. To gain a more comprehensive understanding of the rippling mechanisms, a chemomechanical simulation was conducted during the first two cycles in both 2DSi@C and bare 2DSi for comparison (Figure 3f). The simulation results demonstrate that the 2DSi exhibited much higher first principal stress than the 2DSi@C during the first lithiation, and the stress difference became more conspicuous from the second cycle. The stress analysis indicates that 2DSi@C could relieve the stress by the formation of ripples and demonstrated considerable durability during the cycles. Moreover, the unique structural characteristics of 2DSi@C enable fast ionic transport, showing remarkable performance even at 20 C with 73.9% retention compared to an initial capacity of 0.2 C and 94.9% of capacity retention after 200 cycles at 0.2 C.

## 3. PROGRESS IN MICROSCALE FEATURE SIZE FOR THE PURE SI ANODE

Despite the distinct advantages of nanostructured Si, its practical application has been impeded by inherent drawbacks such as low tap density, poor Coulombic efficiency, and intricate synthesis. Therefore, the development of microstructures that possess the properties of nanoscale Si holds great significance and practical value.

### 3.1. Constructing the Microstructure of the Si Anode

Fabricating nanostructures into microscale secondary particles has been intensively developed to efficiently circumvent the limitations of nanostructured Si while retaining their advantages.[36] An interesting microscale silicene flower (SF) was reported which comprised silicene nanoplates with different orientations that are inherently interconnected, forming a 3D flower-like structure (Figure 4a).[37] The SF design allows for the accommodation of volume changes during cycling, limiting variable SEI formation for improved interfacial stability, attributed to the structural advantages of 2D Si. In addition, the shortened Li-ion diffusion length and interconnected nature of the nanoplates promote robust electron and Li-ion transport channels. The flower-like configuration provides the material with high tap density, which is crucial for practical applications. Nevertheless, the direct contact between the electrolyte and Si could form an unstable SEI layer and induce morphological deformation. Hence, a carbon-coated SF (SF@G) with 2D covalent encapsulation was fabricated which demonstrated stable, high-capacity, and high-rate lithium storage properties.[38] The covalent binding between the native oxide layer of Si and graphene (Si−O−C) enables robust and efficient contact between Si and the formation of an electrically conductive network. The interfacial analysis revealed that the SEI formed on the cycled SF@G composite predominantly consisted of organic compounds with the minimal presence of inorganic materials. The organic-based SEI exhibited greater stability compared to inorganic−organic mixed SEI, rigorously preventing the irreversible consumption of lithium and subsequent SEI formation.

Designing a micrometer-sized 3D porous structure of Si has attracted great interest as another approach due to its mitigated volume expansion effect and fast Li-ion transport kinetics. Several methods have been suggested for producing porous materials based on Si, such as magnesiothermic reduction,[39] metal-assisted chemical etching,[40] dealloying of bulk Si metal alloys,[41] and template-assisted processes.[42] Despite various strategies, microscale 3D porous Si usually exhibits a low tap density owing to its porous nature. As a breakthrough to achieving high tap density in microscale 3D porous Si, ant-nest-like microscale porous Si (AMPSi) was designed which comprised 3D interconnected Si nanoligaments and a bicontinuous nanoporous network (Figure 4b).[43] The unique interconnected structure of AMPSi was confirmed by synchrotron radiation tomographic images and electron images. Such an ingenious design of AMPSi demonstrated a high tap density of 0.84 g $cm^{-3}$ and a high areal capacity of 5.1 mAh $cm^{-2}$ (2.9 mg $cm^{-2}$) with a low electrode swelling ratio of 17.8%. This work, based on the economic and scalable top-down fabrication method, manifests its effectiveness for industrial applications and offers insights into the rational design of a micrometer-sized 3D porous structure of Si.

Microstructured Si can also be constructed through the thermochemical process of $SiO_2$ reduction to Si. Interestingly, an auxiliary $AlCl_3$ molten salt can absorb the generated heat during a typical thermochemical process, while directly participating in the reduction reaction.[44] Using a low-temperature aluminothermic reduction reaction (LTARR) with an $AlCl_3$ molten salts medium, a micrometer-sized hollow porous Si sphere (HPSS) was synthesized at a low reduction temperature (<250 °C) (Figure 4c).[45] The carbon-coated HPSS (HPSS@C) electrodes exhibited outstanding electrochemical performance for 800 cycles without any structural degradation. The remarkable stability of HPSS@C was derived from the presence of a porous shell and a core void available in a microparticle, which can alleviate the significant volume changes that occur in Si anodes during cycling. In situ TEM analysis was conducted to confirm the capability of HPSS@C to accommodate volume changes. In the fully lithiated state of HPSS@C, the shell experienced a 22% expansion, leading to the transformation of the originally porous shell into a dense structure with high contrast, effectively filling both meso- and macropores. Interestingly, the filled pores were able to be restored after the delithiation process, while the shells remained slightly expanded at 17% and maintained their structural integrity. The molten salt medium from LTARR allows the uniform doping of heteroatoms into the Si crystal. For instance, sulfur atoms were homogeneously doped into microsized Si, resulting in a significant enhancement of bulk conductivity, up to 50 times higher than that of undoped Si.[3] The electrode with quasi-metallic Si retained 72% of its initial capacity over 500 cycles at 0.5 C (1 C = 1.9 mAh $cm^{-2}$) along with a high average Coulombic efficiency of 99.89% from the 2nd to 500th cycle. Recently, mixed amorphous−crystalline Si (MACS) microparticles from waste borosilicate glass were


https://doi.org/10.1021/acs.accounts.3c00308
Acc. Chem. Res. 2023, 56, 2213−2224

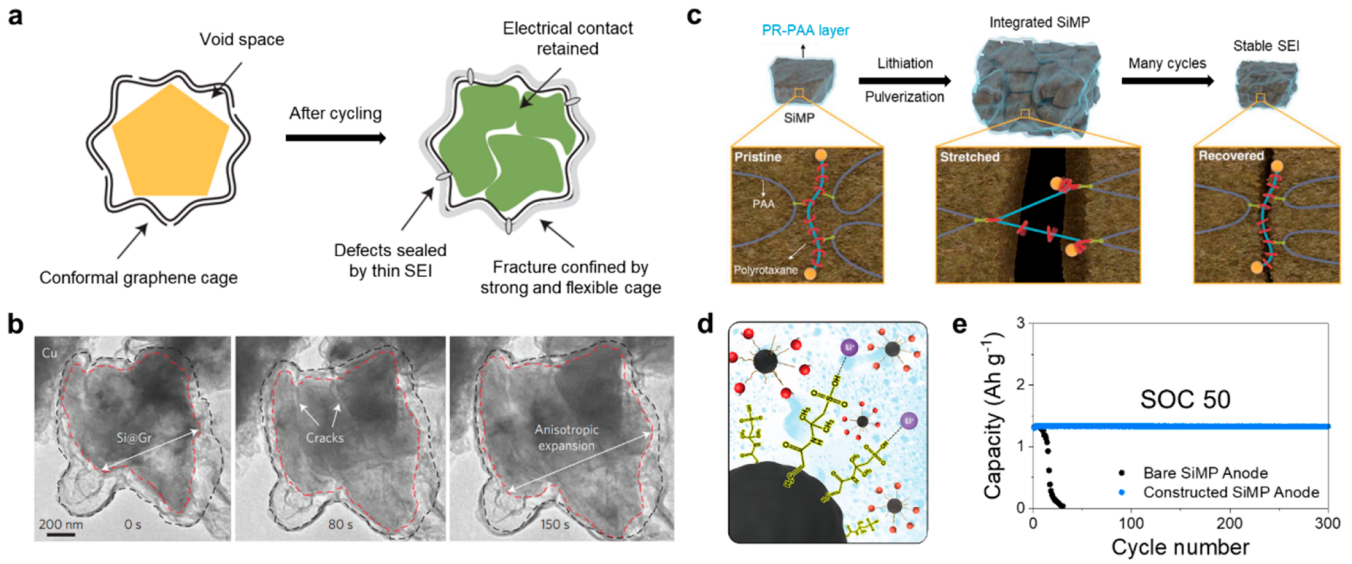


**Figure 5.** Bulk Si engineering for the advanced SiMP anode. (a) Schematic for the reliable structure of graphene cage-encapsulated SiMP after cycling. (b) In situ TEM time-lapse images of graphene cage-encapsulated SiMP during lithiation. Reproduced with permission from ref 48. Copyright 2016 Springer Nature. (c) Graphical representation of the operation of the PR-PAA binder to dissipate the stress during repeated volume changes of SiMPs. Reproduced with permission from ref 53. Copyright 2017 American Association for the Advancement of Science. (d) Schematic illustration of an integrated binder-conductive material system through functionalization. (e) Lithiation limited cycling of the bare SiMP anode and constructed SiMP anode at 0.5 C with state-of-charge (SOC) control to 50%.

fabricated through the LTARR system to achieve a cost-effective and mass-producible process.[4] During the reduction process of waste borosilicate glass, a localized internetwork with disordered atomic bridges of boron (B) and oxygen (O) is formed in the Si crystal (Figure 4d). The MACS not only effectively mitigates the volume changes during cycles but a partially disordered atomic array expands the interspaces within the Si crystal, facilitating fast charging and an extended battery lifespan. The feasibility of mass production was confirmed by using a custom-made liter-scale reactor. This research suggests a comprehensive and scalable methodology for the production and synthesis of versatile Si structures at a micrometer scale.

### 3.2. Constructing the Si Microparticle Anode

While the microstructure of Si exhibited decent performance, the advantages of bulk Si microparticles (SiMPs), such as cost-effectiveness and high energy density, continued to command market attention from a commercial perspective.[46] Significantly, the hoop stress exerted by volume expansion increases proportionally with the size of the Si particles. Bulk SiMPs, being much larger than the threshold size of 150 nm, exceed both the yield strength and the ultimate strength, thereby resulting in the occurrence of fracture and pulverization. Besides, the SiMPs remain vulnerable to fracture despite the implementation of stress mitigation strategies, thus pulverization in SiMP inevitably begins to manifest as the cycling progresses.[47]

Material design for bulk SiMP should regulate the electrical isolation of fractured SiMPs from delamination and side reactions with the electrolyte due to the exposure of fresh surfaces through continuous fracturing. Cui's group applied the concept for nano/microstructuring of an encapsulation strategy to micrometer-sized Si by layering conformal graphene cages with etching-induced void space on the bulk Si (Figure 5a).[48] Confining the SiMPs in the mechanically strong and flexible graphene cage with an ultrathin (~10 nm) thickness rendered a sturdy structure where fragments of Si were physically sealed in the multilayer while retaining the electrical connection and a reliable SEI. Moreover, the internal void created between the SiMP and the graphene cage resulted in decreased stress infliction, demonstrating superior stability of the pure SiMP anode with a comparable loading mass (Figure 5b). Nevertheless, it is difficult to inhibit a series of destructive reactions perfectly arising from the rupture of SiMPs and the SEI layer. Therefore, multifarious and comprehensive approaches should be essential to suppressing the severe volume expansion at both particle and electrode levels, which assists in sustaining structural integrity even when Si particles are fractured.

At the microscale level, the volume expansion of SiMPs cannot be fully averted due to the generation of significantly greater stress. Therefore, synergistic methods have been required to delay Si fracture and efficiently repair the damaged structure. Importantly, the binder within the electrode can engage in direct adhesion with Si particle surfaces owing to the presence of a native oxide layer and polar functional groups on the particle, which contributes to the mechanical properties of Si electrodes.[49] Among various types of binder-mediated interactions, the ionic/dipole interaction has been extensively employed for the binder in Si electrodes, and poly(acrylic acid) (PAA) binder is recognized as a notable representative.[50] The interaction can foster strong supramolecular interaction and even self-healing properties against repeated volume changes.[51] Functionalization or modification of chemical groups in the binder can further improve the electrochemical performance.[52] Choi et al. developed a covalently integrated PAA binder with ring-slide polyrotaxane, which ensured extraordinary elasticity and thus underwent stress dissipation for SiMP (Figure 5c).[53] The rings in polyrotaxane can move freely to lower the tension exerted on the polymer network. Besides, polyrotaxane between PAA chains can hold and recover the Si surface by providing highly stretchable and elastic properties during


https://doi.org/10.1021/acs.accounts.3c00308
Acc. Chem. Res. 2023, 56, 2213−2224

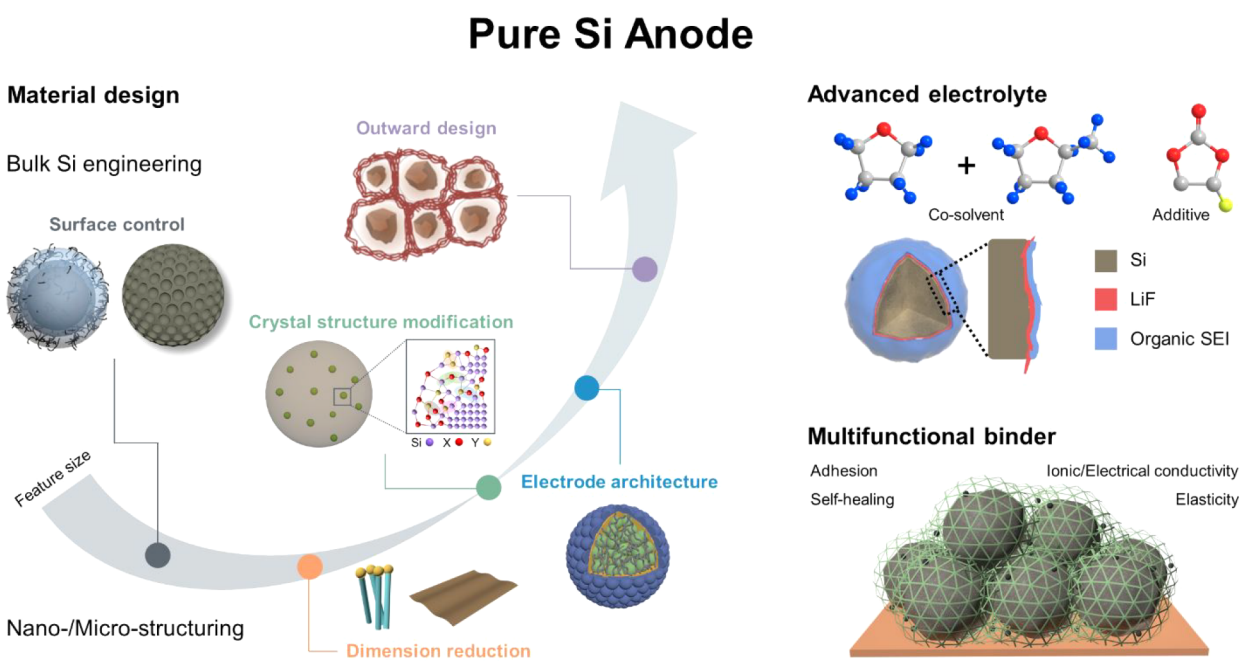


**Figure 6.** Outlook and perspective to achieve a practical pure Si anode for advanced batteries. Adapted with permission from ref 57. Copyright 2020 the authors. Published by Elsevier under a Creative Commons Attribution 4.0 International (CC BY 4.0) License; ref 58, copyright 2021 the authors. Published by Oxford University Press under a Creative Commons CC BY License.

cycling, which causes even fractured and pulverized Si particles to remain coalesced without disintegration. The introduction of the sliding motion of polyrotaxane achieves stable cycle retention with practical mass loading through wide access of the binder combination.

SiMPs, presenting smaller surface area than nanoscale Si, offer fewer reaction sites for charge carriers along with inherent electrical conductivity limitations. Such characteristics facilitate the generation of intensive strain energy as the Li ion accumulates near the surface. In addition, the issues are further exacerbated in the ultrathick film of electrodes for the practical pure Si anode.[54] The challenges can be addressed by modifying the surfaces of the conductive agents, which can enhance the electrical conductivity and reduce interfacial resistance for Si particles (Figure 5d). Functionalization of hydrophilic groups on the conductive agent surface enables the formation of an integrated system with a mechanically excellent binder.[55] The uniformly dispersed conductive material ensures ionic conductivity and fast Li-ion diffusion in a water-based environment.[56] It allows the electrode to meet industry requirements and deliver enhanced electrochemical behavior even in the thick film with a high loading level for the SiMP anode. Furthermore, lithiation-limited cycling of Si materials notably decreases the stress through state-of-charge (SOC) control, enabling the extended battery cycle life in the pouch-type full-cell configuration (Figure 5e). To address the issues associated with SiMPs, comprehensive strategies beyond material design have been employed. The synergistic approaches propose practical solutions, paving a feasible pathway toward the realization of a pure bulk SiMP anode.

## 4. SUMMARY AND PERSPECTIVES

In this Account, we present a comprehensive review of the progress made in the material design of pure Si anodes for advanced batteries. Multifarious strategies related to bulk Si engineering and nano/microstructuring have been explored to stabilize Si electrodes (Figure 6). At the nanoscale, it is crucial to manipulate Si particles to be smaller than a specific size (<150 nm) to avoid pulverization. After reducing the particle size to the nanoscale, various approaches have been employed for engineering SiNPs, including the synthesis of porous or heteroatom-doped SiNPs and coating strategies on SiNP to address challenges related to poor electrical conductivity and an unstable SEI layer.[57] For further enhancement of the electrical conductivity and structural integrity of a pure Si anode, nanostructured Si has been intensively studied. Representative nanostructures such as Si NWs (1D), Si nanosheets (2D), and yolk−shell structures (3D) highlight their distinctive structural benefits, demonstrating their capacity to accommodate volume changes. Although the nanoscale engineering of Si particles can alleviate the volume change and improve electrical conductivity, practical application in LIBs is hindered by inherent challenges, such as low tap density and complex synthesis processes. Consequently, an ingenious material design for microscale Si has recently been developed. Microstructuring of the Si anode has been achieved using diverse approaches, such as hierarchical structures composed of nanosized building blocks, 3D porous structures, and crystal structure modifications. These tactics ensured outstanding electrochemical performance as well as a high tap density. In recent efforts to achieve pure Si anodes toward commercialization, bulk SiMPs have been employed due to their cost-effectiveness and high tap density. A significant breakthrough in this context has been the integration of graphene cages into bulk SiMPs, offering a novel and convenient pathway for practical applications.[58] Moving forward, further research should prioritize the exploration of innovative Si architectures that exhibit high tap density while minimizing particle-level expansion, enabling the attainment of high volumetric energy density. In this regard, achieving a uniform stress distribution and outward expansion throughout the entire microparticle is crucial, making the ingenious design


https://doi.org/10.1021/acs.accounts.3c00308
Acc. Chem. Res. 2023, 56, 2213−2224

of the spatial and pore distribution of the Si component pivotal.

Although, multidirectional methodologies for the material design of Si have been introduced to mitigate the longstanding challenges associated with Si since the early 2000s, relying solely on Si material design is insufficient to fabricate a flawless pure Si anode for advanced batteries. Thus, it is crucial to pay more attention to supplementary materials other than Li host materials (e.g., binder, conductive agent, and electrolyte), which play a distinctive role in promoting the formation of a stable SEI layer and enhancing the structural integrity and conductivity of the electrode. One potential solution is to develop a multifunctional binder that can facilitate the transport of ions while maintaining strong binding with the active material, which enables fabricating the electrodes with high mass loading.[59] For instance, nanoscale Si affords a substantial surface area, which facilitates numerous covalent attachments between native silanol groups on the Si surface and functionalized binder materials.[60] A supramolecular binder network, capable of effectively buffering volume expansion through hydrogen bonding, or a hierarchically ordered conductive binder also constitutes a viable strategy.[61,62] For further improvement, employing carbon nanotubes (CNT) in conjunction with carbon black during the fabrication of electrodes can significantly enhance the electrical conductivity, preventing the isolation of carbon black particles. A segregated network composite incorporating carbon nanotubes ensured the fabrication of ultrathick Si electrodes which can significantly increase the conductivities and lower charge-transfer resistances.[63] Meanwhile, advanced electrolytes offer another potential solution by formulating a stable interface between Si particles and the electrolyte. The well-designed SEI accommodates the large volume change of Si and suppresses the further decomposition of electrolytes, resulting in extending the cycle life.[64,65] Furthermore, solid-state electrolytes such as the gel polymer electrolyte (GPE) can serve as a physical cushion to mitigate the Si expansion during electrochemical cycling, allowing the electrode to recover the original structure.[66] Therefore, it is crucial to integrate Si material design with the exploration of supplementary materials to achieve pure Si anodes for advanced batteries.

## AUTHOR INFORMATION


### Corresponding Authors

**Jaegeon Ryu** − *Department of Chemical and Biomolecular Engineering, Sogang University, Seoul 04107, Republic of Korea;* orcid.org/0000-0002-5290-6192; Email: jryu@sogang.ac.kr

**Soojin Park** − *Department of Chemistry, Pohang University of Science and Technology (POSTECH), Pohang 37673, Republic of Korea;* orcid.org/0000-0003-3878-6515; Email: soojin.park@postech.ac.kr

### Authors

**Minjun Je** − *Department of Chemistry, Pohang University of Science and Technology (POSTECH), Pohang 37673, Republic of Korea*

**Dong-Yeob Han** − *Department of Chemistry, Pohang University of Science and Technology (POSTECH), Pohang 37673, Republic of Korea*

Complete contact information is available at: https://pubs.acs.org/10.1021/acs.accounts.3c00308


### Author Contributions

M.J.: conceptualization (lead), writing − original draft (lead), and writing − review and editing (lead). D.-Y.H.: conceptualization (lead), writing − original draft (lead), and writing − review and editing (lead). J.R.: conceptualization (supporting), supervision (supporting), and writing − review and editing (lead). S.P.: conceptualization (supporting), funding acquisition (lead), supervision (lead), and writing − review and editing (supporting). CRediT: **Soojin Park** conceptualization (lead), funding acquisition (lead), project administration (lead), supervision (lead), writing-original draft (lead), writing-review & editing (lead); **Minjun Je** investigation (equal), validation (equal), writing-original draft (equal), writing-review & editing (equal); **Dong-Yeob Han** conceptualization (equal), investigation (equal), validation (equal), writing-original draft (equal), writing-review & editing (equal); **Jaegeon Ryu** conceptualization (equal), funding acquisition (lead), project administration (equal), validation (equal), writing-original draft (lead), writing-review & editing (equal).

### Author Contributions

[§]M.J. and D.-Y.H. contributed equally to this work. CRediT: **Soojin Park** conceptualization (lead), funding acquisition (lead), project administration (lead), supervision (lead), writing-original draft (lead), writing-review & editing (lead); **Minjun Je** investigation (equal), validation (equal), writing-original draft (equal), writing-review & editing (equal); **Dong-Yeob Han** conceptualization (equal), investigation (equal), validation (equal), writing-original draft (equal), writing-review & editing (equal); **Jaegeon Ryu** conceptualization (equal), funding acquisition (lead), project administration (equal), validation (equal), writing-original draft (lead), writing-review & editing (equal).

### Notes

The authors declare no competing financial interest.

### Biographies

**Minjun Je** received his B.S. degree in 2019 from the School of Energy and Chemical Engineering at Ulsan National Institute of Science and Technology (UNIST). He is currently a Ph.D. candidate in the Department of Chemistry at Pohang University of Science and Technology (POSTECH). His research focuses on the design of alloying-type materials for advanced lithium batteries.

**Dong-Yeob Han** received his B.S. degree in 2019 from the School of Energy and Chemical Engineering at Ulsan National Institute of Science and Technology (UNIST). He is currently a Ph.D. candidate in the Department of Chemistry at Pohang University of Science and Technology (POSTECH). His research focuses on polymer design for next-generation rechargeable batteries.

**Jaegeon Ryu** received his Ph.D. from UNIST in 2018. After postdoctoral research experience at POSTECH and Pacific Northwest National Laboratory for 3 years, he joined the Department of Chemical and Biomolecular Engineering at Sogang University in 2022. He specializes in the development of electrode materials and electrolytes for high-performance next-generation beyond-Li rechargeable batteries.

**Soojin Park** received his Ph.D. in chemistry from Pohang University of Science and Technology (POSTECH) in Korea. After he spent 3 years as a postdoctoral research associate at the University of Massachusetts at Amherst, he joined Ulsan National Institute of Science and Technology (UNIST) in 2009 and moved to the Department of Chemistry at Pohang University of Science and



https://doi.org/10.1021/acs.accounts.3c00308
Acc. Chem. Res. 2023, 56, 2213−2224

Technology (POSTECH) in 2018. His research interests include the design of high-capacity anode materials, polymeric materials for energy storage applications, and next-generation rechargeable batteries.

## ■ ACKNOWLEDGMENTS

S.P. acknowledges support from the National Research Foundation of Korea (NRF) funded by the Ministry of Science and ICT (2023R1A2C2003939). J.R. acknowledges support from the National Research Foundation of Korea (NRF) funded by the Ministry of Science and ICT (2015M3D3A1A01064929).

## ■ ABBREVIATIONS

Li, lithium; SEI, solid−electrolyte interphase; LIBs, lithium ion batteries; NCM811, $LiNi_{0.8}Co_{0.1}Mn_{0.1}O_2$; Si, silicon; $Li_xSi_y$, lithiated Si; SiNPs, silicon nanoparticles; $Li_2SiO_3$ and $Li_2Si_2O_5$, lithium silicate; $Li_4Ti_5O_{12}$, lithium titanate; $E_{insertion}$, Li insertion energy; Ge, germanium; 1D, one-dimensional; 2D, two-dimensional; 3D, three-dimensional; SiNWs, silicon nanowires; TEM, transmission electron microscopy; SAED, selected-area electron diffraction; 2DSi@C, 2D Si nanosheets conformally coated with amorphous carbon layers; SF, silicene flower; SF@G, carbon-coated SF; AMPSi, Ant-nest-like microscale porous Si; LTARR, low-temperature aluminothermic reduction reaction; HPSS, hollow porous Si sphere; HPSS@C, carbon-coated HPSS; B, boron; O, oxygen; P, phosphorus; MACS, mixed amorphous−crystalline Si; SiMPs, silicon microparticles; SOC, state of charge; PAA, poly(acrylic acid); CNT, carbon nanotubes; GPE, gel polymer electrolyte

## ■ REFERENCES

(1) Lee, J.-I.; Ko, Y.; Shin, M.; Song, H.-K.; Choi, N.-S.; Kim, M. G.; Park, S. High-performance silicon-based multicomponent battery anodes produced via synergistic coupling of multifunctional coating layers. *Energy Environ. Sci.* **2015**, *8*, 2075−2084.

(2) Ryu, J.; Chen, T.; Bok, T.; Song, G.; Ma, J.; Hwang, C.; Luo, L.; Song, H.-K.; Cho, J.; Wang, C.; Zhang, S.; Park, S. Mechanical mismatch-driven rippling in carbon-coated silicon sheets for stress-resilient battery anodes. *Nat. Commun.* **2018**, *9*, 2924.

(3) Ryu, J.; Seo, J. H.; Song, G.; Choi, K.; Hong, D.; Wang, C.; Lee, H.; Lee, J. H.; Park, S. Infinitesimal sulfur fusion yields quasi-metallic bulk silicon for stable and fast energy storage. *Nat. Commun.* **2019**, *10*, 2351.

(4) Je, M.; Song, G.; Lee, S.; Park, H. J.; Kim, J.; Park, S. Practical production of heteroatom-bridged and mixed amorphous−crystalline silicon for stable and fast-charging batteries. *J. Mater. Chem. A* **2023**, *11*, 1694−1703.

(5) Armand, M.; Tarascon, J.-M. Building better batteries. *Nature* **2008**, *451*, 652−657.

(6) Dunn, B.; Kamath, H.; Tarascon, J.-M. Electrical Energy Storage for the Grid: A Battery of Choices. *Science* **2011**, *334*, 928−935.

(7) Zhang, H.; Wang, L.; Li, H.; He, X. Criterion for Identifying Anodes for Practically Accessible High-Energy-Density Lithium-Ion Batteries. *ACS Energy Lett.* **2021**, *6*, 3719−3724.

(8) Duffner, F.; Kronemeyer, N.; Tübke, J.; Leker, J.; Winter, M.; Schmuch, R. Post-lithium-ion battery cell production and its compatibility with lithium-ion cell production infrastructure. *Nat. Energy* **2021**, *6*, 123−134.

(9) Wang, L.; Chen, B.; Ma, J.; Cui, G.; Chen, L. Reviving lithium cobalt oxide-based lithium secondary batteries-toward a higher energy density. *Chem. Soc. Rev.* **2018**, *47*, 6505−6602.

(10) Shen, X.; Zhang, X.-Q.; Ding, F.; Huang, J.-Q.; Xu, R.; Chen, X.; Yan, C.; Su, F.-Y.; Chen, C.-M.; Liu, X.; Zhang, Q. Advanced Electrode Materials in Lithium Batteries: Retrospect and Prospect. *Energy Mater. Adv.* **2021**, *2021*, 1205324.

(11) Transparency Market Research, Silicon Anode Lithium-ion Battery Market. https://www.transparencymarketresearch.com/silicon-anode-lithium-ion-battery-market.html.

(12) Shin, W. IBKS Industry Report: Secondary batteries/electronic component (Overweight). http://hkconsensus.hankyung.com/apps.analysis/analysis.downpdf?report_idx=504176.

(13) Greenwood, M.; Wentker, M.; Leker, J. A bottom-up performance and cost assessment of lithium-ion battery pouch cells utilizing nickel-rich cathode active materials and silicon-graphite composite anodes. *J. Power Sources Adv.* **2021**, *9*, 100055.

(14) McDowell, M. T.; Lee, S. W.; Nix, W. D.; Cui, Y. 25th Anniversary Article: Understanding the Lithiation of Silicon and Other Alloying Anodes for Lithium-Ion Batteries. *Adv. Mater.* **2013**, *25*, 4966−4985.

(15) Chan, M. K. Y.; Long, B. R.; Gewirth, A. A.; Greeley, J. P. The First-Cycle Electrochemical Lithiation of Crystalline Ge: Dopant and Orientation Dependence and Comparison with Si. *J. Phys. Chem. Lett.* **2011**, *2*, 3092−3095.

(16) Lee, S. W.; McDowell, M. T.; Choi, J. W.; Cui, Y. Anomalous Shape Changes of Silicon Nanopillars by Electrochemical Lithiation. *Nano Lett.* **2011**, *11*, 3034−3039.

(17) Ryu, I.; Lee, S. W.; Gao, H.; Cui, Y.; Nix, W. D. Microscopic model for fracture of crystalline Si nanopillars during lithiation. *J. Power Sources* **2014**, *255*, 274−282.

(18) Choi, J. W.; Aurbach, D. Promise and reality of post-lithium-ion batteries with high energy densities. *Nat. Rev. Mater.* **2016**, *1*, 16013.

(19) Liu, X. H.; Zhong, L.; Huang, S.; Mao, S. X.; Zhu, T.; Huang, J. Y. Size-Dependent Fracture of Silicon Nanoparticles During Lithiation. *ACS Nano* **2012**, *6*, 1522−1531.

(20) Wortman, J. J.; Evans, R. A. Young's Modulus, Shear Modulus, and Poisson's Ratio in Silicon and Germanium. *J. Appl. Phys.* **1965**, *36*, 153−156.

(21) Kovacs, G. T. A. *Micromachined Transducers Source Book*; McGraw-Hill, Inc.: New York, 1998.

(22) Hertzberg, B.; Benson, J.; Yushin, G. Ex-situ depth-sensing indentation measurements of electrochemically produced Si−Li alloy films. *Electrochem. Commun.* **2011**, *13*, 818−821.

(23) Sethuraman, V. A.; Chon, M. J.; Shimshak, M.; Srinivasan, V.; Guduru, P. R. *In Situ* Measurements of Stress Evolution in Silicon Thin Films During Electrochemical Lithiation and Delithiation. *J. Power Sources* **2010**, *195*, 5062−5066.

(24) Su, X.; Wu, Q.; Li, J.; Xiao, X.; Lott, A.; Lu, W.; Sheldon, B. W.; Wu, J. Silicon-Based Nanomaterials for Lithium-Ion Batteries: A Review. *Adv. Energy Mater.* **2014**, *4*, 1300882.

(25) Ge, M.; Lu, Y.; Ercius, P.; Rong, J.; Fang, X.; Mecklenburg, M.; Zhou, C. Large-Scale Fabrication, 3D Tomography, and Lithium-Ion Battery Application of Porous Silicon. *Nano Lett.* **2014**, *14*, 261−268.

(26) Cheng, Z.; Jiang, H.; Zhang, X.; Cheng, F.; Wu, M.; Zhang, H. Fundamental Understanding and Facing Challenges in Structural Design of Porous Si-Based Anodes for Lithium-Ion Batteries. *Adv. Funct. Mater.* **2023**, *33*, 2301109.

(27) Zhang, C.; Wang, F.; Han, J.; Bai, S.; Tan, J.; Liu, J.; Li, F. Challenges and Recent Progress on Silicon-Based Anode Materials for Next-Generation Lithium-Ion Batteries. *Small Struct.* **2021**, *2*, 2100009.

(28) Long, B. R.; Chan, M. K. Y.; Greeley, J. P.; Gewirth, A. A. Dopant Modulated Li Insertion in Si for Battery Anodes: Theory and Experiment. *J. Phys. Chem. C* **2011**, *115*, 18916−18921.

(29) Domi, Y.; Usui, H.; Shimizu, M.; Kakimoto, Y.; Sakaguchi, H. Effect of Phosphorus-Doping on Electrochemical Performance of Silicon Negative Electrodes in Lithium-Ion Batteries. *ACS Appl. Mater. Interfaces* **2016**, *8*, 7125−7132.

(30) Zhu, B.; Liu, G.; Lv, G.; Mu, Y.; Zhao, Y.; Wang, Y.; Li, X.; Yao, P.; Deng, Y.; Cui, Y.; Zhu, J. Minimized lithium trapping by isovalent isomorphism for high initial Coulombic efficiency of silicon anodes. *Sci. Adv.* **2019**, *5*, eaax0651.



https://doi.org/10.1021/acs.accounts.3c00308
Acc. Chem. Res. 2023, 56, 2213−2224

(31) Ryu, J.; Hong, D.; Shin, M.; Park, S. Multiscale Hyperporous Silicon Flake Anodes for High Initial Coulombic Efficiency and Cycle Stability. *ACS Nano* **2016**, *10*, 10589−10597.
(32) Wang, B.; Ryu, J.; Choi, S.; Zhang, X.; Pribat, D.; Li, X.; Zhi, L.; Park, S.; Ruoff, R. S. Ultrafast-Charging Silicon-Based Coral-Like Network Anodes for Lithium-Ion Batteries with High Energy and Power Densities. *ACS Nano* **2019**, *13*, 2307−2315.
(33) Chan, C. K.; Peng, H.; Liu, G.; McIlwrath, K.; Zhang, X. F.; Huggins, R. A.; Cui, Y. High-performance lithium battery anodes using silicon nanowires. *Nat. Nanotechnol.* **2008**, *3*, 31−35.
(34) Liu, N.; Wu, H.; McDowell, M. T.; Yao, Y.; Wang, C.; Cui, Y. A Yolk-Shell Design for Stabilized and Scalable Li-Ion Battery Alloy Anodes. *Nano Lett.* **2012**, *12*, 3315−3321.
(35) Ryu, J.; Hong, D.; Choi, S.; Park, S. Synthesis of Ultrathin Si Nanosheets from Natural Clays for Lithium-Ion Battery Anodes. *ACS Nano* **2016**, *10*, 2843−2851.
(36) Liu, N.; Lu, Z.; Zhao, J.; McDowell, M. T.; Lee, H.-W.; Zhao, W.; Cui, Y. A pomegranate-inspired nanoscale design for large-volume-change lithium battery anodes. *Nat. Nanotechnol.* **2014**, *9*, 187−192.
(37) Zhang, X.; Qiu, X.; Kong, D.; Zhou, L.; Li, Z.; Li, X.; Zhi, L. Silicene Flowers: A Dual Stabilized Silicon Building Block for High-Performance Lithium Battery Anodes. *ACS Nano* **2017**, *11*, 7476−7484.
(38) Zhang, X.; Wang, D.; Qiu, X.; Ma, Y.; Kong, D.; Müllen, K.; Li, X.; Zhi, L. Stable high-capacity and high-rate silicon-based lithium battery anodes upon two-dimensional covalent encapsulation. *Nat. Commun.* **2020**, *11*, 3826.
(39) Zhang, R.; Du, Y.; Li, D.; Shen, D.; Yang, J.; Guo, Z.; Liu, H. K.; Elzatahry, A. A.; Zhao, D. Highly Reversible and Large Lithium Storage in Mesoporous Si/C Nanocomposite Anodes with Silicon Nanoparticles Embedded in a Carbon Framework. *Adv. Mater.* **2014**, *26*, 6749−6755.
(40) Lee, J.-I.; Lee, K. T.; Cho, J.; Kim, J.; Choi, N.-S.; Park, S. Chemical-Assisted Thermal Disproportionation of Porous Silicon Monoxide into Silicon-Based Multicomponent Systems. *Angew. Chem., Int. Ed.* **2012**, *51*, 2767−2771.
(41) Sohn, M.; Lee, D. G.; Park, H.-I.; Park, C.; Choi, J.-H.; Kim, H. Microstructure Controlled Porous Silicon Particles as a High Capacity Lithium Storage Material via Dual Step Pore Engineering. *Adv. Funct. Mater.* **2018**, *28*, 1800855.
(42) Kim, H.; Han, B.; Choo, J.; Cho, J. Three-Dimensional Porous Silicon Particles for Use in High-Performance Lithium Secondary Batteries. *Angew. Chem., Int. Ed.* **2008**, *47*, 10151−10154.
(43) An, W.; Gao, B.; Mei, S.; Xiang, B.; Fu, J.; Wang, L.; Zhang, Q.; Chu, P. K.; Huo, K. Scalable synthesis of ant-nest-like bulk porous silicon for high-performance lithium-ion battery anodes. *Nat. Commun.* **2019**, *10*, 1447.
(44) Lin, N.; Han, Y.; Zhou, J.; Zhang, K.; Xu, T.; Zhu, Y.; Qian, Y. A low temperature molten salt process for aluminothermic reduction of silicon oxides to crystalline Si for Li-ion batteries. *Energy Environ. Sci.* **2015**, *8*, 3187−3191.
(45) Song, G.; Ryu, J.; Kim, J. C.; Lee, J. H.; Kim, S.; Wang, C.; Kwak, S. K.; Park, S. Revealing salt-expedited reduction mechanism for hollow silicon microsphere formation in bi-functional halide melts. *Commun. Chem.* **2018**, *1*, 42.
(46) Song, G.; Kwak, M.-J.; Hwang, C.; An, C.; Kim, S.; Lee, S.; Choi, S.; Song, H.-K.; Jang, J.-H.; Park, S. Stress-Relief Network in Silicon Microparticles and Composite Anodes for Durable High-Energy-Density Batteries. *ACS Appl. Energy Mater.* **2021**, *4*, 10050−10058.
(47) Zhu, G.; Chao, D.; Xu, W.; Wu, M.; Zhang, H. Microscale Silicon-Based Anodes: Fundamental Understanding and Industrial Prospects for Practical High-Energy Lithium-Ion Batteries. *ACS Nano* **2021**, *15*, 15567−15593.
(48) Li, Y.; Yan, K.; Lee, H.-W.; Lu, Z.; Liu, N.; Cui, Y. Growth of conformal graphene cages on micrometre-sized silicon particles as stable battery anodes. *Nat. Energy* **2016**, *1*, 15029.
(49) Kwon, T.-w.; Choi, J. W.; Coskun, A. The emerging era of supramolecular polymeric binders in silicon anodes. *Chem. Soc. Rev.* **2018**, *47*, 2145−2164.
(50) Parikh, P.; Sina, M.; Banerjee, A.; Wang, X.; D'Souza, M. S.; Doux, J.-M.; Wu, E. A.; Trieu, O. Y.; Gong, Y.; Zhou, Q.; Snyder, K.; Meng, Y. S. Role of Polyacrylic Acid (PAA) Binder on the Solid Electrolyte Interphase in Silicon Anodes. *Chem. Mater.* **2019**, *31*, 2535−2544.
(51) Ryu, J.; Kim, S.; Kim, J.; Park, S.; Lee, S.; Yoo, S.; Kim, J.; Choi, N.-S.; Ryu, J.-H.; Park, S. Room-Temperature Crosslinkable Natural Polymer Binder for High-Rate and Stable Silicon Anodes. *Adv. Funct. Mater.* **2020**, *30*, 1908433.
(52) Jung, C.-H.; Kim, K.-H.; Hong, S.-H. Stable Silicon Anode for Lithium-Ion Batteries through Covalent Bond Formation with a Binder via Esterification. *ACS Appl. Mater. Interfaces* **2019**, *11*, 26753−26763.
(53) Choi, S.; Kwon, T.-w.; Coskun, A.; Choi, J. W. Highly elastic binders integrating polyrotaxanes for silicon microparticle anodes in lithium ion batteries. *Science* **2017**, *357*, 279−283.
(54) Eshetu, G. G.; Zhang, H.; Judez, X.; Adenusi, H.; Armand, M.; Passerini, S.; Figgemeier, E. Production of high-energy Li-ion batteries comprising silicon-containing anodes and insertion-type cathodes. *Nat. Commun.* **2021**, *12*, 5459.
(55) Gong, C.; Xue, Z.; Wang, X.; Zhou, X.-P.; Xie, X.-L.; Mai, Y.-W. Poly(ethylene glycol) grafted multi-walled carbon nanotubes/LiFe-$PO_4$ composite cathodes for lithium ion batteries. *J. Power Sources* **2014**, *246*, 260−268.
(56) Kuratani, K.; Ishibashi, K.; Komoda, Y.; Hidema, R.; Suzuki, H.; Kobayashi, H. Controlling of Dispersion State of Particles in Slurry and Electrochemical Properties of Electrodes. *J. Electrochem. Soc.* **2019**, *166*, A501−A506.
(57) Li, G.; Huang, L.-B.; Yan, M.-Y.; Li, J.-Y.; Jiang, K.-C.; Yin, Y.-X.; Xin, S.; Xu, Q.; Guo, Y.-G. An integral interface with dynamically stable evolution on micron-sized $SiO_x$ particle anode. *Nano Energy* **2020**, *74*, 104890.
(58) Chen, F.; Han, J.; Kong, D.; Yuan, Y.; Xiao, J.; Wu, S.; Tang, D.-M.; Deng, Y.; Lv, W.; Lu, J.; Kang, F.; Yang, Q.-H. 1000 Wh $L^{-1}$ lithium-ion batteries enabled by crosslink-shrunk tough carbon encapsulated silicon microparticle anodes. *Natl. Sci. Rev.* **2021**, *8*, nwab012.
(59) Han, D.-Y.; Han, I. K.; Son, H. B.; Kim, Y. S.; Ryu, J.; Park, S. Layering Charged Polymers Enable Highly Integrated High-Capacity Battery Anodes. *Adv. Funct. Mater.* **2023**, *33*, 2213458.
(60) Kwon, T.-w.; Jeong, Y. K.; Lee, I.; Kim, T.-S.; Choi, J. W.; Coskun, A. Systematic Molecular-Level Design of Binders Incorporating Meldrum's Acid for Silicon Anodes in Lithium Rechargeable Batteries. *Adv. Mater.* **2014**, *26*, 7979−7985.
(61) Cho, Y.; Kim, J.; Elabd, A.; Choi, S.; Park, K.; Kwon, T.-w.; Lee, J.; Char, K.; Coskun, A.; Choi, J. W. A Pyrene-Poly(acrylic acid)-Polyrotaxane Supramolecular Binder Network for High-Performance Silicon Negative Electrodes. *Adv. Mater.* **2019**, *31*, 1905048.
(62) Zhao, Y.; Coskun, A. Heating up the binder. *Nat. Energy* **2023**, *8*, 113−114.
(63) Park, S.-H.; King, P. J.; Tian, R.; Boland, C. S.; Coelho, J.; Zhang, C.; McBean, P.; McEvoy, N.; Kremer, M. P.; Daly, D.; Coleman, J. N.; Nicolosi, V. High areal capacity battery electrodes enabled by segregated nanotube networks. *Nat. Energy* **2019**, *4*, 560−567.
(64) Chen, J.; Fan, X.; Li, Q.; Yang, H.; Khoshi, M. R.; Xu, Y.; Hwang, S.; Chen, L.; Ji, X.; Yang, C.; He, H.; Wang, C.; Garfunkel, E.; Su, D.; Borodin, O.; Wang, C. Electrolyte design for LiF-rich solid−electrolyte interfaces to enable high-performance microsized alloy anodes for batteries. *Nat. Energy* **2020**, *5*, 386−397.
(65) Park, S.; Jeong, S. Y.; Lee, T. K.; Park, M. W.; Lim, H. Y.; Sung, J.; Cho, J.; Kwak, S. K.; Hong, S. Y.; Choi, N.-S. Replacing conventional battery electrolyte additives with dioxolone derivatives for high-energy-density lithium-ion batteries. *Nat. Commun.* **2021**, *12*, 838.


https://doi.org/10.1021/acs.accounts.3c00308
Acc. Chem. Res. 2023, 56, 2213−2224

(66) Huang, Q.; Song, J.; Gao, Y.; Wang, D.; Liu, S.; Peng, S.; Usher, C.; Goliaszewski, A.; Wang, D. Supremely elastic gel polymer electrolyte enables a reliable electrode structure for silicon-based anodes. *Nat. Commun.* **2019**, *10*, 5586.



https://doi.org/10.1021/acs.accounts.3c00308
*Acc. Chem. Res.* 2023, 56, 2213−2224